

Metal-insulator transition in CuIr_2S_4 : XAS results on the electronic structure

M. Croft,^{1,2} W. Caliebe,² H. Woo,³ T. A. Tyson,³ D. Sills,¹ Y. S. Hor,¹ S-W. Cheong,¹ V. Kiryukhin,¹ and S-J. Oh^{1,*}

¹*Department of Physics and Astronomy, Rutgers University, Piscataway, New Jersey 08854*

²*Brookhaven National Laboratory, Upton, New York 11973*

³*Department of Physics, New Jersey Institute of Technology, Newark, New Jersey 07102*

(Received 18 March 2003; published 20 May 2003)

S K and Ir L_3 x-ray absorption measurements across the temperature-induced metal (M) to insulator (I) transition in CuIr_2S_4 are presented. Dramatic S K -edge changes reflect the Ir d -electronic state redistribution across this transition. These changes, along with a detailed consideration of the I -phase structure, motivate a model in which the I -phase stabilization involves an interplay of charge and d -orbital orientation ordering along Ir chains, a quadrupling of the Ir-chain repeat unit, and correlated dimer spin-singlet formation.

DOI: 10.1103/PhysRevB.67.201102

PACS number(s): 71.30.+h, 78.70.Dm

Metal-insulator transitions involving transition metal (T) compounds have been of intense interest in recent years on both fundamental and technological grounds.^{1,2} This field has been dominated by $3d$ -row T -oxide compounds, by virtue of the renaissance in these materials that followed the discovery of high- T_c superconductivity.³ The subclass of mixed valent metallic compounds that “charge order” into an insulating state has been the focus of special recent interest.² The compound CuIr_2S_4 stands out as unique in this subclass for a number of reasons.^{4–9}

The spinel structure CuIr_2S_4 compound has a paramagnetic, high-temperature, homogeneously mixed $\text{Ir}^{3+}/\text{Ir}^{4+}$, metallic (M) phase, which undergoes a first-order transition (near 230 K) to a low-temperature, charge-ordered, diamagnetic, insulating (I) phase.^{4–9} Recent definitive x-ray and neutron scattering measurements showed this I phase to involve a complex ordering of Ir^{4+} -spin-singlet dimers and undimerized Ir^{3+} sites.¹⁰ This finding is novel, since such dimerization transitions have previously occurred almost exclusively in compounds with clearly defined quasi-one-dimensional (1D) chains, and certainly not in a complex three-dimensional (3D) type structure.¹¹ Moreover, the complex pairwise ordering of Ir^{3+} - Ir^{3+} nondimer and Ir^{4+} - Ir^{4+} singlet-dimer moieties appears not to have been previously observed. In addition, the broadness of the $5d$ orbitals makes such M - I transitions rare in $5d$ -row compounds, and still rarer in a nonoxide (i.e., S) $5d$ compound. These properties, along with the previous dearth of precise structural or electronic information, have hindered the development of the outlines of a theory for the M - I transition in CuIr_2S_4 . In this paper, we present S and Ir XAS results spanning the M - I transition in CuIr_2S_4 . The S K -edge results, along with a careful review of the dimerized/charge-ordered chain character of the I phase, motivate a proposal for a specific electronic/structural basis from which to approach understanding of this novel I - M transition.

The sample preparation and characterization techniques were as discussed in Ref. 10. The S K and Ir L_3 XAS measurements were, respectively, performed on beamlines X19A and X18B at the Brookhaven National Synchrotron Light Source, using methods discussed in Refs. 12 and 13. The low-temperature XAS measurements on X19A utilizes a nitrogen cryostat (in the fluorescence mode), and those on

X18B used a displax refrigerator (using the transmission mode).

Previous photoemission spectroscopy measurements on CuIr_2S_4 showed a subtle loss of electronic states at 0.2 eV below the Fermi energy (E_F) in the I phase.⁶ These photoemission and I -phase inverse photoemission results manifested substantial departures⁶ from band-structure predictions⁹ on a wider energy scale. Thus the generic gap formation below E_F , and the absence of any information about above- E_F density-of-state (DOS) changes across this M - I transition, have provided little guidance to direct the theoretical attack on this interesting system.

XAS has been important in elucidating atomic/orbital-specific electronic structure in many classes of transition metal compounds. The combination of O K -edge (probing O p states) and Cu $L_{2,3}$ -edge (probing Cu d states) measurements emphasized the crucial importance of hybridized O p /Cu d hole states in the physics of high- T_c cuprates.¹⁴ Importantly, O K -edge measurements on VO_2 clarified the specific electronic structure changes behind its metal to dimerized-insulator transition.¹⁵ Systematic O K -edge measurements in $T(3d)$ -O compounds have profiled (via their threshold structure) the important variations in their hybridized O p /T d empty states.¹⁶ $4d/5d$ -hole states have been studied extensively by T $L_{2,3}$ -edge spectroscopy in transition-metal compounds.¹² Finally, T($3d$) K -edge XAS has been used to chronicle the valence variations in manganites and the charge donation to Cu in electron-doped high- T_c materials.¹³ This background motivates our S K - and Ir L_3 -edge studies across the M - I phase transition in CuIr_2S_4 . Cu K -edge measurements in our laboratory, along with previous NMR⁵ and band-structure⁹ calculations, indicate a d^{10} Cu^{1+} state in CuIr_2S_4 , allowing us to neglect Cu d state influences on the S states above E_F .

The elemental S K edge in Fig. 1(a) is dominated by an intense “white line” (WL) feature, due to dipole transitions into empty $3p$ states. In transition-metal sulfide compounds, one typically observes¹⁷ a diminution of the WL intensity due to T to S charge transfer and the appearance of prominent threshold features, shifted down by 0–5 eV from the elemental-S WL, due to hybridized S p /T d states. The S K threshold features probe the T(d) DOS (weighted by transi-

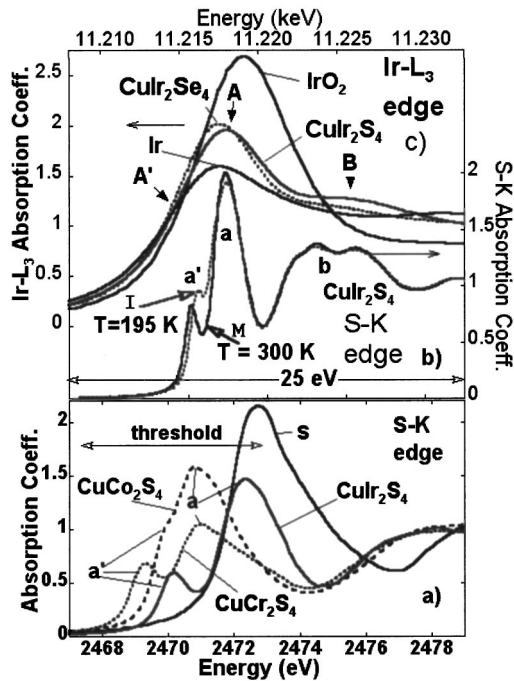


FIG. 1. (a) The S *K* edges of elemental S and CuT_2S_4 , with $T = \text{Cr, Co, and Ir}$. The a' - and a -threshold features are, respectively, associated with $T d t_{2g}$ and e_g state hybridization. (b) The S *K* edges of CuIr_2S_4 , at temperatures $T = 195 \text{ K}$ (in the *I* phase) and 300 K (in the *M* phase). (c) The Ir L_3 edges of elemental Ir, IrO_2 , CuIr_2Se_4 , and CuIr_2S_4 . The intensity in the A and A' positions are associated with Ir $d t_{2g}$ and e_g final states, respectively.

tion matrix element effects) in sulfides in the same sense as O *K* threshold features do in oxides.¹⁶ The S *K*-edge spectra for the spinel compounds CuT_2S_4 ($T = \text{Cr, Co, and Ir}$) in Fig. 1(a) illustrate this for the octahedral ligand field case, where the d orbitals are split into a lower t_{2g} sextet and an upper e_g quartet. For the isoelectronic $3d$ Co and $5d$ Ir compounds, the empty states are $t_{2g}^{0.5}e_g^4$ and for the Cr compound they are $t_{2g}^{2.5}e_g^4$. The a and a' features in the S *K* spectra are associated with the empty S p states, hybridized with the empty t_{2g} and e_g states, respectively. Consistent with band calculations,⁹ the ligand field splitting for $T = \text{Ir}$ is large (yielding a resolved $a' - a$ splitting) and smaller for the more localized Co d orbitals (yielding an unresolved a' shoulder on the a feature). In the $T = \text{Cr}$ case, the broader d bands and larger number of t_{2g} holes broaden the threshold features and enhance the a' -feature intensity. Finally, although not germane to this work, it should be noted that a full treatment of such threshold features should include exchange and multiplet effects, particularly for the Cr compound.

Figure 1(b) compares the S *K*- and Ir L_3 -edge spectra on the same (albeit displaced) energy scale for the *I* and *M* phases of CuIr_2S_4 . The Ir L_3 edge also manifests an intense WL feature due to the $5d$ states above E_F . The A feature, at the L_3 edge of CuIr_2S_4 , involves the four empty e_g states per Ir, and the aligned S *K* a peak is associated with the transitions to S p /Ir $d(e_g)$ hybridized states. The $\frac{1}{2}t_{2g}$ hole per Ir makes a weak unresolved contribution to the Ir L_3 WL near the A' energy range; however, the S *K* a' feature, involving

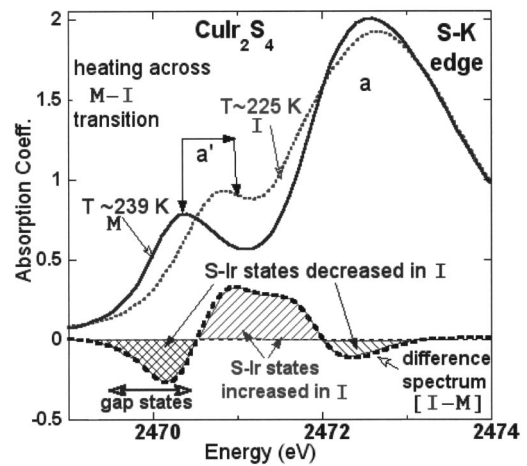


FIG. 2. Comparison of the S *K* edges of CuIr_2S_4 just across the *I*-phase (225 K) to *M*-phase (239 K) transition. The difference (bottom) between the *I*- and *M*-phase spectra is shown to highlight the full details of the *M* to *I* electronic state changes.

S p /Ir $d(t_{2g})$ hybridized states, defines these t_{2g} states much more sharply. The alignment of the Ir L_3 B feature and S *K* b feature for the CuIr_2S_4 suggests S-Ir hybridization effects at these higher energies.¹²

For comparison, the Ir L_3 edges of IrO_2 , CuIr_2Se_4 , and Ir metal are also shown in Fig. 1(c). The higher WL intensity and chemical shift of the IrO_2 spectrum reflect its higher valence relative to CuIr_2S_4 . The Ir L_3 spectrum of CuIr_2Se_4 shows a greater Ir d DOS near E_F , relative to CuIr_2S_4 , consistent with a higher density of overlapping states near E_F in the always-metallic Se isomorph.⁶ The combination of monochromator resolution, core hole broadening, and core-hole/ d -electron interactions make the Ir L_3 WL feature essentially identical in the *M* and *I* phases of CuIr_2S_4 .

S *K*-edge spectra were taken as the sample slowly warmed through the *I*-*M* transition (with temperature measurements being $\pm 5 \text{ K}$) and the details of the discontinuous spectral change can be seen by comparing the $T \sim 225 \text{ K}$ *I*-phase and $T \sim 239 \text{ K}$ *M*-phase spectra in Fig. 2 (top). The difference between these spectra, shown in Fig. 2 (bottom) provides a direct estimate of the detailed Ir d /S- p state redistribution occurring at the transition. Here we will focus only on the central element of this redistribution, the dramatic shift of the $a'(t_{2g})$ feature to higher energy in the *I* phase. A proper theoretical treatment of this transition should also replicate the state redistribution on the low energy side of the a feature.

We tacitly assume the S *K* threshold features are dominated by electronic structure effects in analogy to all past O *K*-edge threshold measurements.¹⁴⁻¹⁶ The close quantitative similarity of our *I*-phase S *K* threshold spectra to the *I*-phase inverse photoemission results⁶ strongly supports this assumption.

We will pattern our proposals for understanding CuIr_2S_4 after those of the Abbate *et al.*¹⁵ reformulation of Goodenough's ideas¹⁸ for the paramagnetic-metal-to-dimerized-insulator transition in VO_2 . These authors^{15,18} developed a simple molecular orbital (MO) theory for VO_2 , motivated by

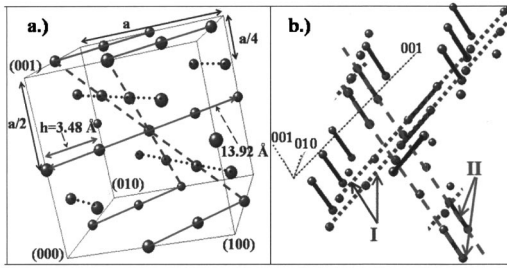


FIG. 3. (a) The Ir atoms (only) in the cubic spinel CuIr_2S_4 . Note the interleaved and Ir-chain structure and threefold chain intersections at the Ir sites (see center Ir). (b) The *I*-phase Ir chains of CuIr_2S_4 with surrounding atoms omitted for clarity. The isolated circles are Ir^{3+} and the circles, connected by heavy lines, are Ir^{4+} - Ir^{4+} dimers. Class *I* chains (light dotted line) are along the triclinic-($1\bar{1}0$) direction with the Ir^{4+} - Ir^{4+} - Ir^{3+} - Ir^{4+} interatomic distances being 3.06, 3.59, 3.66, and 3.59 Å and the chain repeat distance being 13.95 Å. Class *II* chains (light dashed line) are along the $(01\bar{1})$ direction with the interatomic distances being 3.00, 3.72, 3.55, and 3.66 Å and the chain repeat distance being 13.93 Å.

the appearance of a prominent *OK* threshold feature in the *I* phase. The model was based on a strong hybridization-induced splitting of dimer *V* *d* states (d_{\parallel} states) oriented along the chains of edge-sharing VO_6 octahedra in the rutile structure.^{15,18} Abbate *et al.*¹⁵ noted, and Sommers *et al.*¹⁹ emphasized, that Mott-Heitler-London electron correlation effects also contribute to the d_{\parallel} splitting.

The spinel structure of CuIr_2S_4 is decidedly three dimensional, however, as Fig. 3(a) illustrates, it also contains crisscrossing Ir chains with an Ir-Ir spacing of $h=3.48$ Å = $a\sqrt{2}/4$, where *a* is the lattice parameter. The chains cross in adjacent planes *a/2* apart, and cross-linking chains create three-fold chain intersections at the Ir sites (see the cube center). The cell edge-to-edge chain has a length of $4h=13.92$ Å and contains four Ir atoms in the cubic cell. In the metallic phase the $\text{Ir}^{3.5+}$ atoms, with a configuration of $t_{2g}^{5.5}$, can be thought of as $[t_{2g}^4][t_{2g}^{1.5}]$, where the former bracket constitutes two filled *d* orbitals and the latter a $\frac{3}{4}$ -filled band for the highest-lying $d(t_{2g})$ orbital.

Space limitations preclude detailed discussion of the complex triclinic ($a=11.95$ Å, $b=6.98$ Å, $c=11.93$ Å, $\alpha=91.05^\circ$, $\beta=108.47^\circ$, and $\gamma=91.03^\circ$) *I*-phase structure;¹⁰ however, several crucial points should be noted [see Fig. 3(b)]. All Ir atoms are members of charge-ordered $\dots\text{Ir}^{3+}\text{Ir}^{4+}\text{Ir}^{4+}\text{Ir}^{3+}\dots$ chains with dimerized Ir^{4+} - Ir^{4+} pairs. There are two closely related types of chains (*I* and *II*) having unit repeat distances of $\sim 4h$, and extending along approximately orthogonal triclinic cell edge-to-edge directions. Planes of chains in these two directions alternate in the third direction. At staggered chain crossing regions, adjacent Ir^{3+} - Ir^{4+} atoms are still close (in the 3.43–3.56 Å range); however, the orientation of the crucial near- E_F , *d*-orbital charge lobes, within our model, should be *along the chains*. This should produce minimal overlap between the filled-shell t_{2g}^6 Ir^{3+} on one chain, and the transverse *d* lobe on the Ir^{4+} on the adjacent chain, leading to near- E_F *d* bands with quasi-1D character (within a 3D geometrical structure).

The four atom repeat unit in the *I*-phase chains is com-

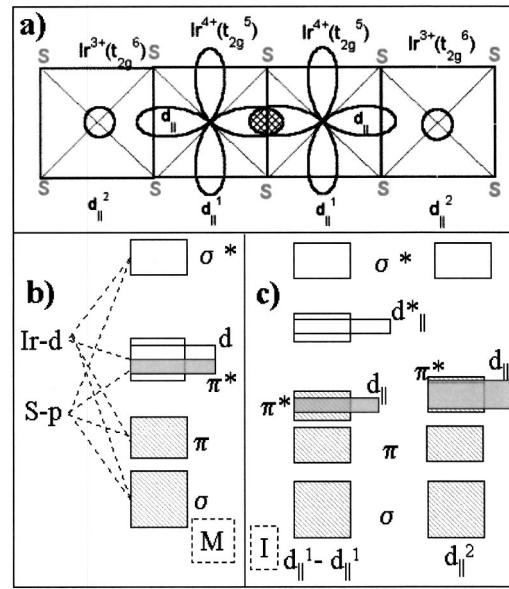


FIG. 4. Schematic views of the proposed electronic properties of CuIr_2S_4 . (a) The *I*-phase chain repeat unit with IrS_6 octahedra being viewed from above. The overlapping d_{\parallel}^1 orbital lobes of the Ir^{4+} dimer are shown. The filled d_{\parallel}^2 shell Ir^{3+} sites are represented by circles. (b) The proposed MO electronic structure in the *M* phase. (c) The proposed MO electronic structure, in the *I* phase at the dimerized (left) and undimerized (right) sites. Note only the highest lying t_{2g} *d* states have been shown explicitly in the diagram.

posed of a t_{2g}^5 - t_{2g}^5 dimer, bounded by two filled-orbital t_{2g}^6 sites. After Abbate *et al.*,¹⁵ we denote the last filled *d* orbital along the chain as d_{\parallel} and note that the *I*-phase chain sequence would be $d_{\parallel}^2 d_{\parallel}^1 - d_{\parallel}^1 d_{\parallel}^2$. In the extended-zone scheme, the dispersion curve for the d_{\parallel} band would now have new gaps at $\pi/4h$, $\pi/2h$, and $3\pi/4h$. The $3\pi/4h$ gap falls in the range of the Fermi energy of the $\frac{3}{4}$ filled d_{\parallel} band, and the removal of nested states near E_F should play some role in the *M* to *I* transition. Sommers *et al.*¹⁹ emphasized that electron repulsion/correlation effects were important in VO_2 , along with direct d_{\parallel} overlap effects. We believe the correlated singlet dimerization energy is crucial here also, and while the direct *d*-overlap effects should be enhanced and the correlation effects reduced in this 5*d* Ir compound, both are anticipated.

In Fig. 4(a) we show a schematic representation of the dimer-containing chain repeat cell indicating the filled d_{\parallel}^2 sites with circles, and the oriented d_{xy} -type charge cloud¹⁰ at the d_{\parallel}^1 sites. The intersite direct d_{\parallel}^1 - d_{\parallel}^1 overlap of the dimer, across the shared octahedral edge, is emphasized.

In the *M* phase of CuIr_2S_4 , the itinerant *d* holes are hopping on and off Ir sites along three-fold cross-linked chains, with the spatial orientation of the d_{xy} charge lobes also fluctuating. The transition to the *I* phase involves several components: a $\text{Ir}^{3+}\text{Ir}^{4+}\text{Ir}^{4+}\text{Ir}^{3+}$ charge ordering with a concomitant quadrupling of the chain cell to $\sim 4h$, an orbital ordering of the charge lobes at each site into one chain and across the shared edge of an Ir^{4+} - Ir^{4+} dimer, and finally, d_{\parallel}^1 - d_{\parallel}^1 hybridization into a spin singlet dimer with correlation effects.

In Fig. 4(b) the MO proposal for the *M* phase of CuIr_2S_4 is shown. The bonding (σ)–antibonding (σ^*) orbitals involve Ir $d(e_g)$ states that point toward the S sites, and induce strongly split hybrid states. The less split bonding (π)–antibonding (π^*) orbitals involve Ir d states that point between the S sites, and hybridize more weakly. The highest-lying Ir $d(t_{2g})$ orbital [labeled d in Fig. 4(b)] is partially filled at E_F .

In the *I* phase there will be two differing MO combinations, one for the $d_{\parallel}^1-d_{\parallel}^1$ dimer and one for the d_{\parallel}^2 sites which are shown in Fig. 4(c). At the dimer site, the splitting of the d states into a bonding d_{\parallel} and antibonding d_{\parallel}^* pair is dramatic. The fact that both the d_{\parallel}^* and d_{\parallel} states carry hybridized S- p states with them, away from E_F , has been emphasized in Fig. 4(c) by the additional broader box accompanying these states. At the Ir^{3+} d_{\parallel}^2 site, the closed d_{\parallel}^2 orbital falls below E_F . Thus in this MO model the *M-I* transition involves; the redistribution of the near- E_F states in the *M* phase, into the *I*-phase dimer site bonding/antibonding ($d_{\parallel}/d_{\parallel}^*$) states, and into the filled t_{2g} states at the Ir^{3+} site.

Referring back to our S *K*-edge results in Fig. 2, in the *M* phase we associate the high-lying MO σ^* states and the near- E_F MO π^* d states with the S *K a* and *a'* features, respectively. In the *I* phase, the *a* feature and σ^* states persist relatively unchanged in both the S-*K* edge results and MO model. The shift of the *a'* feature to higher energy in the *I* phase is associated with the splitting of the MO antibond-

ing d_{\parallel}^* states to above E_F at the dimer sites. The bonding d_{\parallel} states at the dimer sites, and the filled t_{2g} states at the Ir^{3+} sites, are both pulled below E_F and do not contribute to the S *K* edge. Thus, this simple starting-point model involves the *I* phase arising from orbital ordering of the d -orbital charge lobes into in-chain d_{\parallel} states, and intrachain charge ordering into Ir^{4+} - Ir^{4+} ($d_{\parallel}^1-d_{\parallel}^1$) correlated singlet dimers bounded by Ir^{3+} filled d_{\parallel}^2 orbital sites.

More generally, the underlying electronic origin of the *M-I* transition in this system appears, at present, unique among 5*d* row compound. Besides explaining our XAS results, the proposed MO picture appears to explain the photoemission gap formation below E_F . Interestingly, the fact that the band structure calculation predicts a metallic state, even in a tetragonally distorted phase (Ref. 9), strongly suggests that the electrons in the *I* phase have localized character, despite the common belief that 5*d* electrons form broad bands. Hence, the *MI* transition would appear to involve electron localization due to correlation effects.

ACKNOWLEDGMENTS

This work was supported by the DOE under NSLS Contract No. DE-AC02-98CH10886, the NSF under Grants No. DMR-0093143 and No. DMR-0103858, and the Korean Science and Engineering Foundation through CSCMR.

*Permanent address: Department of Physics and Center for Strongly Correlated Materials Research, Seoul National University, Seoul 151-742 Korea.

¹M. Imada, *Rev. Mod. Phys.* **70**, 1039 (1998).

²M. Salamon and M. Jaime, *Rev. Mod. Phys.* **73**, 583 (2001).

³J. Bednorz and K. Muller, *Rev. Mod. Phys.* **60**, 585 (1988).

⁴T. Furubayashi *et al.*, *J. Phys. Soc. Jpn.* **63**, 3333 (1994).

⁵K. Kumagai *et al.*, *Physica C* **341**, 741 (2000).

⁶J. Matsuno *et al.*, *Phys. Rev. B* **55**, R15 979 (1997).

⁷S. Nagata *et al.*, *Phys. Rev. B* **58**, 6844 (1998).

⁸A. T. Burkov *et al.*, *Phys. Rev. B* **61**, 10 049 (2000).

⁹T. Oda *et al.*, *J. Phys.: Condens. Matter* **7**, 4433 (1995).

¹⁰P. Radaelli *et al.*, *Nature (London)* **416**, 155 (2002).

¹¹See G. Grüner, *Density Waves in Solids* (Addison-Wesley, Reading, 1994).

¹²See J. Chen *et al.*, *Phys. Rev. B* **46**, 15 639 (1992) and Y. Jeon *et al.*, *ibid.* **50**, 6555 (1994), and references therein

¹³See M. Croft *et al.*, *Phys. Rev. B* **55**, 8726 (1997) and J. M. Tranquada *et al.*, *Nature (London)* **337**, 720 (1989).

¹⁴C. T. Chen *et al.*, *Phys. Rev. Lett.* **68**, 2543 (1992).

¹⁵M. Abbate *et al.*, *Phys. Rev. B* **43**, 7263 (1991).

¹⁶F. M. F. de Groot *et al.*, *Phys. Rev. B* **40**, 5715 (1989).

¹⁷See J. Yan *et al.*, *J. Alloys Compd.* **229**, 216 (1995) and G. Huffman *et al.*, *Energy Fuels* **5**, 574 (1991).

¹⁸J. B. Goodenough, *J. Solid State Chem.* **3**, 490 (1971).

¹⁹C. Sommers *et al.*, *Solid State Commun.* **28**, 133 (1978).